

AN IMPLEMENTATION OF ROTOR SPEED OBSERVER FOR SENSORLESS INDUCTION MOTOR DRIVE IN CASE OF MACHINE PARAMETER UNCERTAINTY

Hau Huu VO¹, Pavel BRANDSTETTER², Tinh Cong TRAN³, Chau Si Thien DONG¹

¹Department of Control & Automation, Faculty of Electrical and Electronics Engineering, Ton Duc Thang University, 19 Nguyen Huu Tho Street, Tan Phong Ward, District 7, Ho Chi Minh City, Vietnam

²Department of Electronics, Faculty of Electrical Engineering and Computer Science, VSB–Technical University of Ostrava, 17. listopadu 15, 708 00 Ostrava, Czech Republic

³Department of Electronics & Telecommunications Engineering, Faculty of Electrical and Electronics Engineering, Ton Duc Thang University, 19 Nguyen Huu Tho Street, Tan Phong Ward, District 7, Ho Chi Minh City, Vietnam

vohuuha@tdtu.edu.vn, pavel.brandstetter@vsb.cz, trancongthinh@tdtu.edu.vn, chausithiendong@tdtu.edu.vn

DOI: 10.15598/aece.v16i4.2973

Abstract. *The paper describes observers using model reference adaptive system for sensorless induction motor drive with the pulse width modulator and the direct torque control under the circumstances of incorrect information of induction motor parameters. An approximation based on the definition of the Laplace transformation is used to obtain initial values of the parameters. These values are utilized to simulate sensorless control structures of the induction motor drive in Matlab-Simulink environment. Performance comparison of two typical observers is carried out at different speed areas and in presence of parameter uncertainty. A laboratory stand with the induction motor drive and load unit is set up to verify the properties of observers. Experimental results confirm the expected dynamic properties of selected observer.*

Keywords

Direct torque control, incorrect parameter, induction motor drive, model reference adaptive system, pulse-width modulator, sensorless control.

1. Introduction

The term “sensorless” means that the electric drive does not contain the speed or position sensor in its control structure, and the concept of sensorless control is to use estimation algorithms to obtain rotor speed, ro-

tor position or flux from voltages and currents of motor terminals. These signals are measured using current and voltage sensors, the important parts of the electric drive structure, and processed by suitable observers that are embedded into a real control system with Digital Signal Processor (DSP). The main techniques which are used for rotor speed estimation can be classified as follows:

- Machine model-based methods that include observers: Model Reference Adaptive System (MRAS), Extended Kalman Filter (EKF), Luengerger Observer (LO), Sliding Mode Observer (SMO), etc.
- Methods without machine model that include injection methods and soft computing methods.

The scheme of machine model-based methods is simple and easy to implement into DSPs. However, there are specific demands on these methods from different drives. The popular sensorless method, reference frame or Rotor Flux MRAS (RF-MRAS) observer, is based on the rotor-flux error calculated using two different voltage and current models of the rotor flux [1].

However, the pure integration of the voltage signals particularly at low speeds, and the low accuracy because of machine parameter uncertainties make it difficult-to-implement. Combination of the method and other techniques such as Kalman filter is one of approaches for performance improvement [2]. A sixth-order discrete-time model is used to analysis convergence of the EKFs for sensorless motion control systems

with Induction Motor (IM) [3]. The Luenberger observer can be a replacement for the observers that use machine model, have accuracy problems, especially at low speeds, and for non-linear systems. The deterministic observer comprises the deterministic plant model while the stochastic type comprises other plant model representations, and the Luenberger observer is a typical deterministic observer. The LO for sensorless IM drive is an observer that uses machine model and a feedback loop with measured stator current and rotor flux. However, the gain matrix of the full-order observer must be designed according to Lyapunov's stability theory, and the observer must be faster than the observed system [4].

Another solution is utilization of the SMO. The main difference between LO and SMO is that the error between the stator current and its estimated quantity is replaced by a sliding function of the error in SMO. This sliding function is designed thanks to sliding mode theory for robustness assurance to machine parameter deviations. The sliding-mode component ensures robustness to large parameter variations and measurement noise in combined scheme of SMO and LO [5]. The SMO is used in rotor flux estimation of sensorless IM drive and gives high robustness to saturation of the magnetizing inductance and variation of the rotor resistance [6].

In the stator Current-Based MRAS (CB-MRAS) observer, the estimated value of the stator current is obtained by a model. The difference between the real stator current and its estimated value is used to derive the speed-error correction signal [1]. There is no design of the gain matrix in the observer. The stability analysis of the observer was tested from the point of view of the induction motor and Proportional-Integral (PI) controller parameter changes, on the basis of the observer transfer function. The RF-MRAS, Back ElectroMotive Force MRAS (BEMF-MRAS), CB-MRAS observers were analyzed by simulations and the CB-MRAS scheme was chosen for implementation into real control system because of its good tracking capability [7].

Parameters of an induction motor vary with its working condition, and machine model-based speed observers are sensitive to variations of parameters of induction motor such as the vector control that is very sensitive to variations in the rotor time constant [8]. In general, methods of stator resistance or rotor time constant estimation are based on application of observers, EKFs, MRASs, artificial intelligence [9], [10], [11], [12], [13] and [14]. These methods require complicated design and computing and does not ensure applicability in real system. Therefore, in the paper, an offline identification is done for obtaining initial values of machine parameters. Then these values are used in simulations

to select an observer that has both simple structure and strong robustness to machine parameter deviation.

2. Offline Parameter Identification

In the paper, the following symbols are used: $\vec{u}_s, \vec{i}_s, \vec{\psi}_r$ - respectively stator voltage vector, stator current vector, rotor flux vector in $[\alpha, \beta]$ coordinate system; $u_{s\alpha}, u_{s\beta}$ - components of the stator voltage vector; $i_{s\alpha}, i_{s\beta}$ - components of the stator current vector; $\psi_{r\alpha}, \psi_{r\beta}$ - components of the rotor flux vector; R_s - stator resistance; $L_s, L_{s\sigma}$ - stator inductance, stator leakage inductance; R_r - rotor resistance; $L_r, L_{r\sigma}$ - rotor inductance, rotor leakage inductance; L_m - magnetizing inductance; σ - total leakage constant; T_s, T_r - stator, rotor time constants; ω_r - real rotor angular speed; denotes the estimated values. For induction motor, equivalent circuit of one phase is shown in Fig. 1 where $u(t), i(t)$ are input and output signals, which are the phase stator voltage and the phase stator current respectively. Stator and rotor leakage inductances are respectively defined by following equations:

$$\sigma_s = \frac{L_{s\sigma}}{L_m} = \frac{L_s}{L_m} - 1, \quad (1)$$

$$\sigma_r = \frac{L_{r\sigma}}{L_m} = \frac{L_r}{L_m} - 1. \quad (2)$$

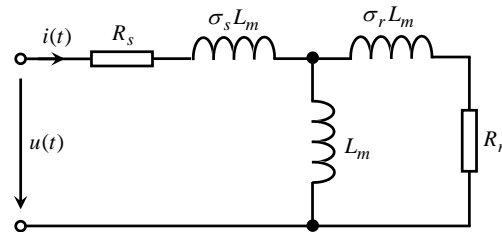


Fig. 1: Equivalent circuit of one phase of an induction motor.

Assume that the circuit is initially relaxed, following equation shows the relation between Laplace transformations of the input and the output [14]:

$$\frac{U(s)}{I(s)} = R_s + s\sigma_s L_m + \frac{(s\sigma_r L_m + R_r) s L_m}{s L_m (\sigma_r + 1) + R_r}. \quad (3)$$

We get the following equation by inserting Eq. (1) and Eq. (2) into Eq. (3):

$$\frac{I(s)}{U(s)} = \frac{1}{R_s} \left[\frac{T_r s + 1}{\sigma T_r T_s s^2 + (T_r + T_s) s + 1} \right]. \quad (4)$$

In case of the phase stator voltage is a constant DC signal, Laplace transformation of the output is calculated according to Eq. (5):

$$I(s) = \frac{U}{R_s} \frac{1}{s} \left[\frac{T_r s + 1}{\sigma T_r T_s s^2 + (T_r + T_s) s + 1} \right], \quad (5)$$

where U is an input DC voltage. The output is obtained by applying the inverse Laplace transform [15] to Eq. (5):

$$i(t) = \frac{U}{R_s} \left[1 + \left(T_r + \frac{1}{X_1} \right) \frac{e^{X_1 t}}{\sqrt{\Delta}} - \left(T_r + \frac{1}{X_2} \right) \frac{e^{X_2 t}}{\sqrt{\Delta}} \right], \quad (6)$$

where:

$$X_1 = \frac{-(T_r + T_s) + \sqrt{\Delta}}{2\sigma T_r T_s}, \quad (7)$$

$$X_2 = \frac{-(T_r + T_s) - \sqrt{\Delta}}{2\sigma T_r T_s}, \quad (8)$$

$$\Delta = (T_r + T_s)^2 - 4\sigma T_r T_s. \quad (9)$$

Experiments with different values of U are carried out. Many methods can be used to approximate IM parameters. For simplicity, the saved data are processed to obtain parameters thanks to the simple approximation of Laplace transform:

$$\hat{I}(s) = \sum_{k=1}^n i(k)e^{-t(k)s} [t(k) - t(k-1)], \quad (10)$$

where n is number of samples of the saved data, k is representative of the k^{th} sample of the time or the phase stator current. Initial values of IM parameters are listed in Tab. 1.

Tab. 1: Initial values of IM parameters.

Parameter	R_s [Ω]	R_r [Ω]	L_s [H]	L_r [H]	L_m [H]
Value	3.179	2.118	0.209	0.209	0.192

3. Model Reference Adaptive System Observers

The structure of RF-MRAS observer is shown in Fig. 2(a). In the reference model or the voltage model, the stator voltage and stator current vectors are used for obtaining rotor flux vector. In the adaptive model or the current model, the estimated rotor flux vector can be gotten from stator current vector together with the estimated value of rotor speed.

The outputs of reference model and adaptive model are calculated according to Eq. (11) and Eq. (12):

$$\vec{\psi}_r = \frac{L_r}{L_m} \left[\int (\vec{u}_s - R_s \vec{i}_s) dt - \frac{L_s L_r - L_m^2}{L_r} \vec{i}_s \right], \quad (11)$$

$$\vec{\psi}_r = \int \left[\left(j\hat{\omega}_r - \frac{1}{T_r} \right) \vec{\psi}_r + \frac{L_m \vec{i}_s}{T_r} \right] dt. \quad (12)$$

The relationship for the rotor speed estimation is calculated according to Eq. (13) and Eq. (14):

$$\xi = \psi_{r\beta} \hat{\psi}_{r\alpha} - \psi_{r\alpha} \hat{\psi}_{r\beta}, \quad (13)$$

$$\hat{\omega}_r = K_P \xi + K_I \int_0^t \xi dt, \quad (14)$$

where ξ is called the adaptive signal, $K_P > 0$, $K_I > 0$. Hyperstability of the RF-MRAS observer can be proved as in [16] thanks to Popov's theorem of hyperstability and asymptotic hyperstability [17], definitions of positive real and strictly positive real transfer function matrix, and strictly positive real transfer function matrix [18]. The system of the observer that consists of Eq. (11), Eq. (12), Eq. (13) and Eq. (14) fulfills conditions of the lemma "Strictly positive real transfer function matrix" because rotor time constant is always larger than zero.

The structure of CB-MRAS observer for the rotor speed estimation is shown in Fig. 2(b). This MRAS observer uses stator currents as output quantities of the reference model. The CB-MRAS scheme has one reference model (stator current of induction motor) and two adaptive models (current estimator and model current).

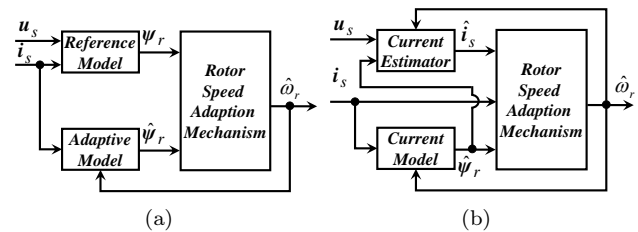


Fig. 2: Structure of (a): RF-MRAS and (b): CB-MRAS observers.

The output of the current estimator, which is the estimated stator current vector, is calculated according to Eq. (15), Eq. (16), Eq. (17), Eq. (18) and Eq. (19):

$$\frac{d}{dt} \vec{i}_s = K_1 \vec{u}_s + K_2 \vec{\psi}_r - jK_3 \hat{\omega}_r \vec{\psi}_r - K_4 \vec{i}_s, \quad (15)$$

$$K_1 = \frac{L_r}{L_s L_r - L_m^2}, \quad (16)$$

$$K_2 = \frac{L_m R_r}{L_r (L_s L_r - L_m^2)}, \quad (17)$$

$$K_3 = \frac{L_m}{L_s L_r - L_m^2}, \quad (18)$$

$$K_4 = \frac{L_m^2 R_r + L_r^2 R_s}{L_r (L_s L_r - L_m^2)}. \quad (19)$$

The current model is identical to the adaptive model which is described by Eq. (12). The relationship for the rotor speed estimation is calculated as follows:

$$\xi = (i_{s\alpha} - \hat{i}_{s\alpha}) \hat{\psi}_{r\beta} - (i_{s\beta} - \hat{i}_{s\beta}) \hat{\psi}_{r\alpha}, \quad (20)$$

$$\hat{\omega}_r = K_P \xi + K_I \int_0^t \xi dt, \quad (21)$$

where ξ is also called the adaptive signal, $K_P > 0$, $K_I > 0$. The global asymptotic stability of the CB-MRAS observer can be proved through the second Lyapunov's method with the same Lyapunov's function candidate, as in the case of LO [19], and there are no requirements in design of gain matrix of the observer. The K_I component in Eq. (14) and Eq. (21) is removed whenever one of two limits of estimated rotor speed is reached because this component has a much larger influence on the observer stability than the K_P one [1].

4. Simulation Results

For high performance applications of IM drives, Vector Control (VC) and Direct Torque Control (DTC) are used for electromagnetic torque control. They can be comparable to each other. The advantage of the DTC methods is that their structures are not as complicated as those of VC methods and therefore, they are easy to implement on DSPs. The utilization of PWM in the DTC structure is to ensure the constant switching frequency. In this section, the PWM-DTC control structure with two MRAS observers were simulated (see Fig. 3). Parameters of induction motor used in simulations were given by Tab. 1. Voltage of DC link is 540 V. Parameters of speed controller are $K_P = 1.5$, $T_I = 0.05$ s, limitation ± 10 N·m. Parameters of PI controllers for two observers are the same, with $K_P = 500$, $T_I = 0.002$ s, limitation ± 200 rpm. The switching frequency is 20 kHz. Time courses of important quantities were obtained from the control structures at the jump of the load torque $T_L = 5$ N·m (see Fig. 4).

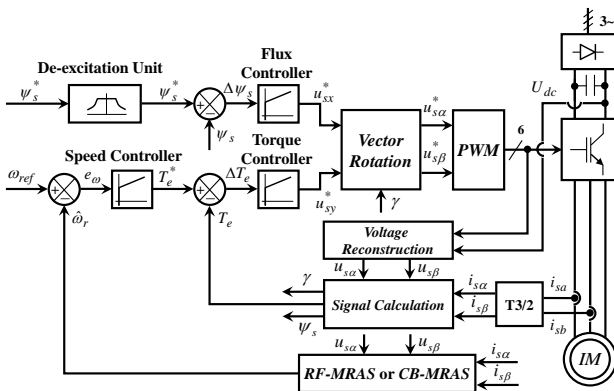


Fig. 3: Sensorless control structure with the PWM-DTC method.

To evaluate the control quality of simulated sensorless IM drive it is important to evaluate the speed responses in different situations. The simulations were performed for the reference speeds which represent two

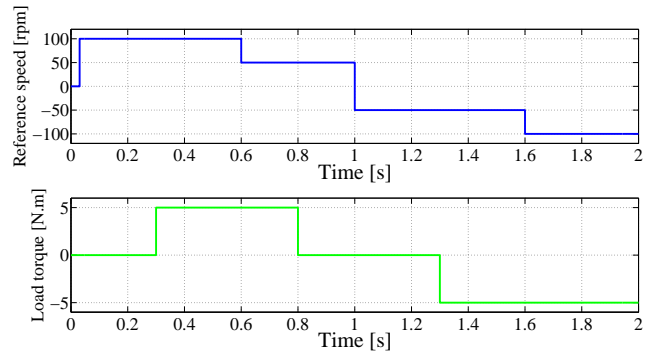


Fig. 4: Reference speed $\omega_{ref} = n(t)$, and load torque.

speed areas: area of low speed ($1.0 \omega_{ref}$) and area of very low speed ($0.1 \omega_{ref}$). Speed deviations are evaluated as follows [7]:

$$\Delta\omega_r = \max(\omega_r - \hat{\omega}_r) \quad [\text{rpm}], \quad (22)$$

$$\delta\omega_r = \frac{\Delta\omega_r}{\omega_r(t_{\Delta\omega})} \quad [-]. \quad (23)$$

The two abbreviations RF and CB respectively denote the RF-MRAS and the CB-MRAS observers. Figure 5, Fig. 6, Fig. 7 and Fig. 8 show real rotor speed, estimated rotor speed, speed difference between real rotor speed and estimated rotor speed at low and very low speed areas. Speed deviations for two speed areas are listed in Tab. 2. Deviations at both dynamic and steady state operations with RF-MRAS are much larger than those with CB-MRAS at two speed areas. A test at usual speed area was also simulated to compare the performance of two observers. Figure 9 claims that RF-MRAS gives speed deviations at both operations larger than CB-MRAS does.

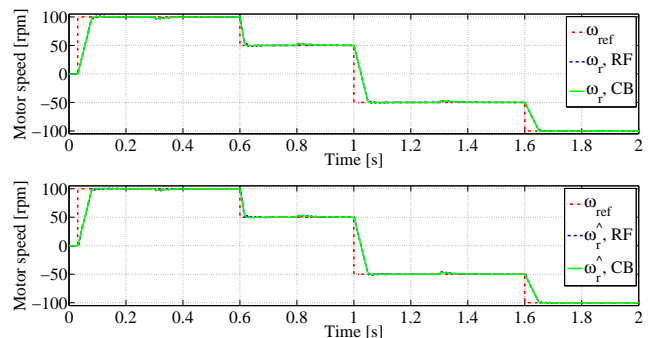


Fig. 5: Real rotor speed (upper) and estimated rotor speed (lower) at low speed area.

The described observers are based on IM model. Hence, it is necessary to consider the sensitivity of the observers with parameter uncertainty. Some simulations are used to check the robust stability of two MRAS observers. Reference speed and load torque at low speed area are the same as those (see Fig. 4) with time range 0 to 0.6 seconds. For simulations, two selected parameters are R_s and T_r (or R_r) with changes from -10% to $+10\%$ of their known values.

Tab. 2: Speed deviations at low speed and very low speed areas.

Operation	Deviation	Low speed area		Very low speed area	
		RF	CB	RF	CB
Dynamic operation	$ \Delta\omega_r $	5.37	0.35	1.96	0.09
	$\delta\omega_r$	0.06	0.004	0.54	0.01
Steady-state operation	$ \Delta\omega_r $	0.26	0.02	0.006	0.003
	$\delta\omega_r$	0.005	0.0004	0.0006	0.0003

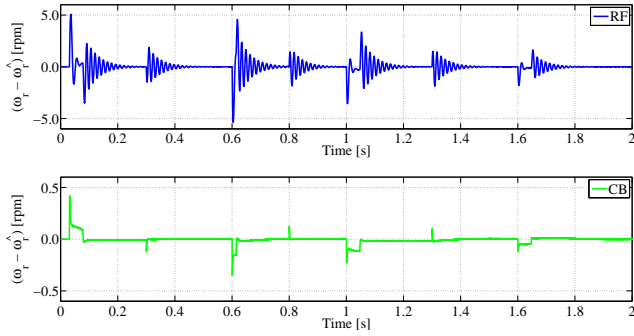


Fig. 6: Speed difference with RF (upper) and CB (lower) at low speed area.

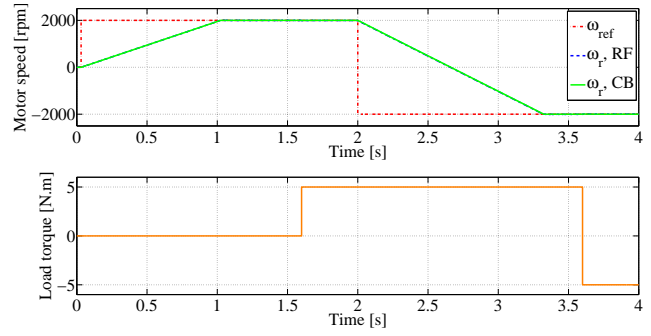


Fig. 9: Speeds (upper) and load torque (lower) at usual speed area.

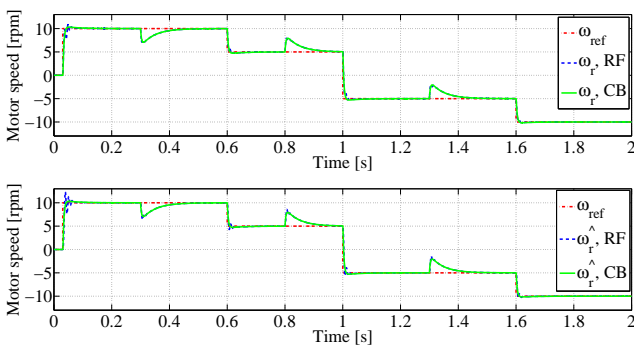


Fig. 7: Real rotor speed (upper) and estimated rotor speed (lower) at very low speed area.

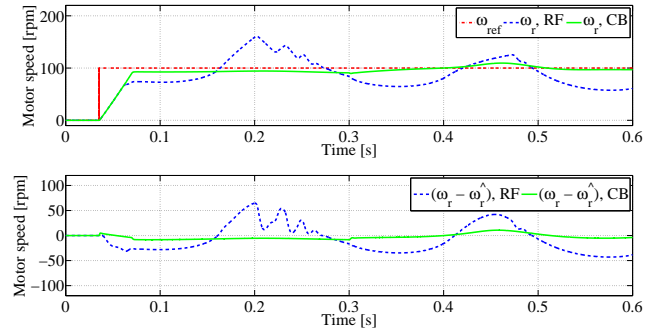


Fig. 10: Real rotor speed (upper) and speed difference (lower) with real values of R_s and T_r decreased 10 % of their known values.

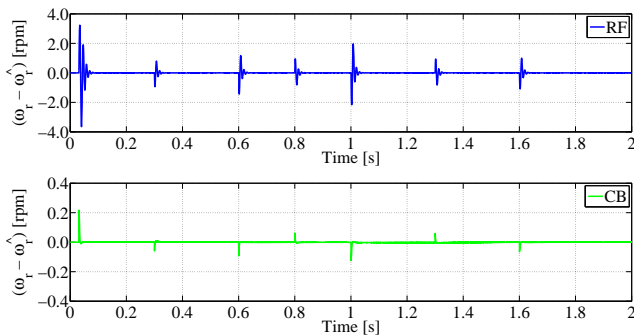


Fig. 8: Speed difference with RF (upper) and CB (lower) at very low speed area.

In case of R_s and T_r decreased by 10 % of their known value, real rotor speed and speed difference are shown in Fig. 10, speed difference with CB-MRAS is significantly smaller than that with RF-MRAS. For comparison, deviations in both dynamic and steady-state operations are listed in Tab. 3, Tab. 4, Tab. 5 and Tab. 6 where smaller deviations are bold.

In most cases, deviations with CB-MRAS are smaller than those with RF-MRAS. Therefore, the CB-MRAS gives better tracking capability at different speed areas and stronger robustness in presence of parameter uncertainty than the RF-MRAS does. Two coefficients K_1 , K_3 are constant with the changes of R_s and R_r . Percentage of changes of coefficients K_2 , K_4 compared to their known values are listed in Tab. 7. It is easy to see that the deviations with CB-MRAS are more affected by coefficient K_4 than by coefficient K_2 . For CB-MRAS, the coefficient K_4 is experimentally adjusted more elaborately than three remaining in next section.

5. Experimental Results

A laboratory workplace with an induction motor and a load unit was used to verify performance of two MRAS observers with PWM-DTC (see Fig. 11). The load unit is an electro-dynamometer with torque range

Tab. 3: Deviation $|\Delta\omega_r|$ in dynamic operation.

		R_s									
		-10 %		-5 %		0 %		5 %		10 %	
		RF	CB	RF	CB	RF	CB	RF	CB	RF	CB
T_r	-10 %	64.7	10.7	19.0	9.4	4.1	14.3	11.8	20.0	21.6	26.0
	-5 %	72.5	17.2	37.5	4.0	4.3	6.8	13.3	13.0	24.2	24.8
	0 %	79.3	20.9	43.8	8.6	5.1	0.4	15.7	8.7	26.7	18.2
	5 %	86.5	26.9	47.4	13.8	12.6	6.4	20.2	3.8	28.9	12.3
	10 %	94.4	37.6	49.6	19.6	18.8	12.2	25.9	6.7	31.1	7.5

Tab. 4: Deviation $\delta\omega_r$ in dynamic operation.

		R_s									
		-10 %		-5 %		0 %		5 %		10 %	
		RF	CB	RF	CB	RF	CB	RF	CB	RF	CB
T_r	-10 %	0.41	0.10	0.16	0.11	0.14	0.21	0.11	0.44	0.21	0.59
	-5 %	0.44	0.19	0.33	0.04	0.49	0.09	0.12	0.53	0.24	0.45
	0 %	0.46	0.21	0.39	0.21	0.53	0.27	0.14	0.05	0.26	0.32
	5 %	0.50	0.26	0.42	0.14	0.12	0.08	0.18	0.04	0.28	0.19
	10 %	0.56	0.36	0.43	0.20	0.20	0.14	0.23	0.07	0.26	0.07

Tab. 5: Deviation $|\Delta\omega_r|$ in steady-state operation.

		R_s									
		-10 %		-5 %		0 %		5 %		10 %	
		RF	CB	RF	CB	RF	CB	RF	CB	RF	CB
T_r	-10 %	43.0	8.3	19.7	5.5	3.7	3.8	7.9	6.0	8.1	8.4
	-5 %	42.2	17.3	19.4	3.5	1.7	1.8	7.5	3.2	9.3	5.7
	0 %	42.3	19.6	23.5	1.6	0.02	0.01	10.4	1.4	13.0	3.6
	5 %	44.9	24.7	25.4	13.6	12.7	1.8	13.2	3.0	16.6	4.4
	10 %	50.1	21.0	28.0	19.0	17.7	3.6	22.4	4.6	20.2	5.9

Tab. 6: Deviation $\delta\omega_r$ in steady-state operation.

		R_s									
		-10 %		-5 %		0 %		5 %		10 %	
		RF	CB	RF	CB	RF	CB	RF	CB	RF	CB
T_r	-10 %	0.75	0.09	0.24	0.06	0.038	0.040	0.09	0.06	0.088	0.090
	-5 %	0.72	0.19	0.24	0.04	0.018	0.019	0.07	0.03	0.09	0.06
	0 %	0.73	0.21	0.21	0.02	0.0002	0.0001	0.09	0.01	0.12	0.03
	5 %	0.80	0.27	0.26	0.14	0.13	0.02	0.12	0.03	0.14	0.04
	10 %	0.99	0.19	0.30	0.19	0.17	0.03	0.20	0.04	0.17	0.06

Tab. 7: Percentage of changes of two coefficients K_2, K_4 compared to their known values.

		R_s									
		-10 %		-5 %		0 %		5 %		10 %	
		K_2	K_4								
T_r	-10 %	11.1	-2.4	11.1	0.8	11.1	4.0	11.1	7.2	11.1	10.4
	-5 %	5.3	-4.5	5.3	-1.3	5.3	1.9	5.3	5.1	5.3	8.3
	0 %	0.0	-6.4	0.0	-3.2	0.0	0.0	0.0	3.2	0.0	6.4
	5 %	-4.8	-8.1	-4.8	-4.9	-4.8	-1.7	-4.8	1.5	-4.8	4.7
	10 %	-9.1	-9.7	-9.1	-6.5	-9.1	-3.3	-9.1	-0.1	-9.1	3.1

Tab. 8: Maximal differences [%] after activation, release of load unit.

	$\omega_{ref} = 250$ rpm	$\omega_{ref} = 100$ rpm	$\omega_{ref} = 25$ rpm
Activation	5.7	5.2	12.4
Release	4.8	6.3	19.6
Jump of load torque	3 N·m	1.5 N·m	0.5 N·m



Fig. 11: Laboratory workplace.

0–3 N·m at speed range 250–3000 rpm. Induction motor is supplied by a frequency converter that consists of IGBTs SKM75GB12V. A belt mechanically connects the induction motor with the load unit. The control of the inverter output voltage is performed by the space vector PWM technique with switching frequency 3.0 kHz. The control voltage amplitude is 10 V. Therefore, transfer constant of the inverter is $0.05774 U_{dc}$. The control system is a TMS320F28335 digital signal processor.

Figure 12 and Fig. 13 show real and estimated rotor speeds, speed difference and motor torque without load at $\omega_{ref} = 100$ rpm. The time courses confirm that speed deviations with CB-MRAS at both dynamic and steady state operations are significantly smaller than those with RF-MRAS. Hence, the CB-MRAS is chosen for experiments with load (see Fig. 14, Fig. 15, Fig. 16 and Fig. 17).

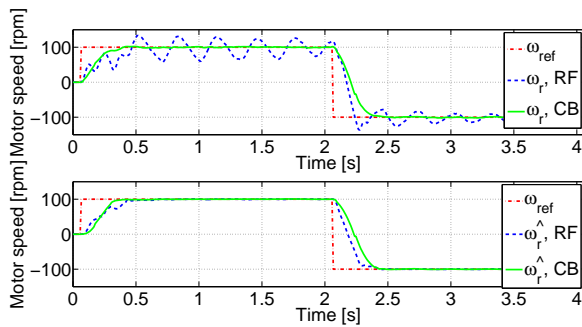


Fig. 12: Real rotor speed (upper) and estimated rotor speed (lower) with two observers at $\omega_{ref} = 100$ rpm.

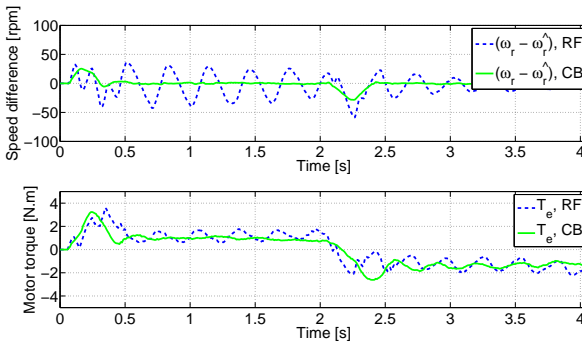


Fig. 13: Speed difference (upper) and motor torque (lower) with two observers at $\omega_{ref} = 100$ rpm.

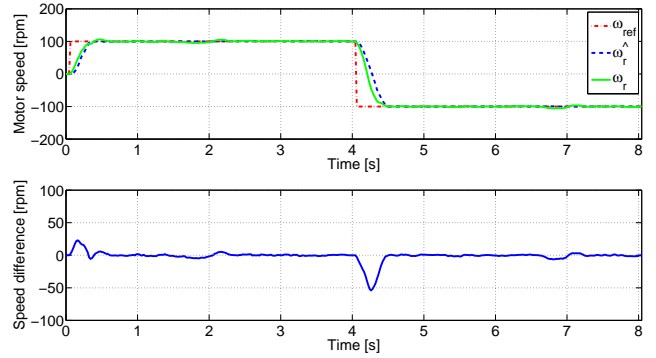


Fig. 14: Laboratory workplace.

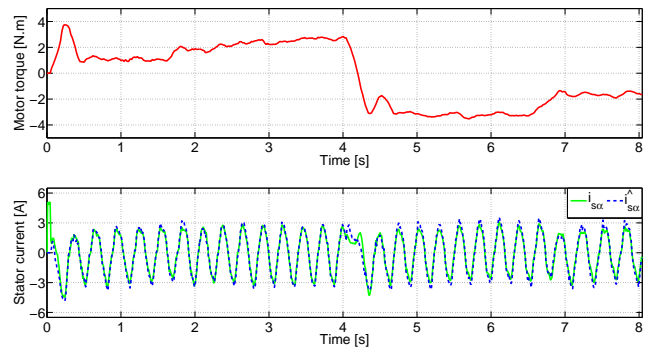


Fig. 15: Real rotor speed (upper) and estimated rotor speed (lower) with two observers at $\omega_{ref} = 100$ rpm.

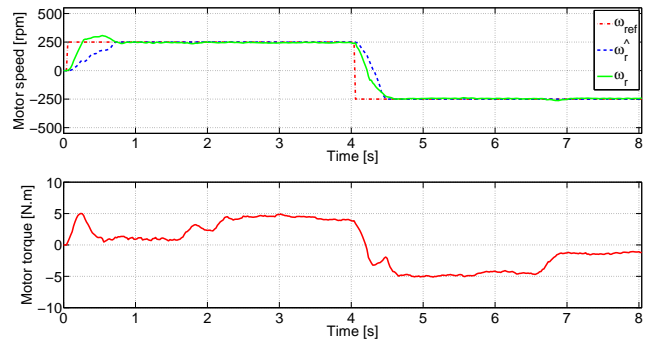


Fig. 16: Motor speeds (upper) and motor torque (lower) with CB-MRAS at $\omega_{ref} = 250$ rpm.

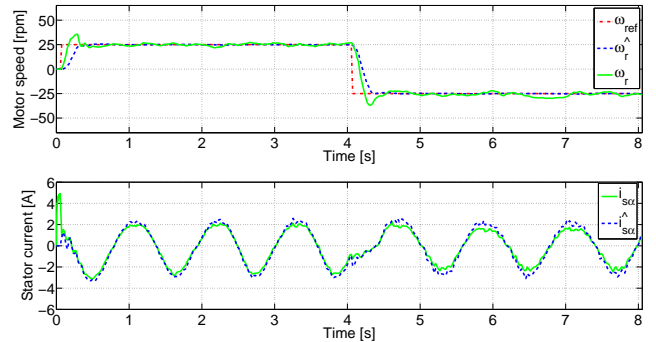


Fig. 17: Motor speeds (upper) and stator current (lower) with CB-MRAS at $\omega_{ref} = 25$ rpm.

Maximal differences after an activation and a release of a load unit are listed in Tab. 8. The differences tend to increase when the speed is lower.

6. Conclusions

The sensorless IM drive using MRAS speed observers with PWM-DTC method were presented in the paper. Simulations were carried out with simultaneous changes of machine parameters to select suitable MRAS observer for implementation on real control system. The IM drive with two MRAS observers gave good dynamic responses and the estimation of the mechanical speed was good in both dynamic and steady-state operations. The CB-MRAS observer gave higher accuracy at different speed areas, and stronger robustness to uncertainty of IM parameters than the RF-MRAS observer. It was the selected solution for sensorless IM drive.

The experimental results with sensorless IM drive using the MRAS observers without load confirmed the assumptions in simulations, and the CB-MRAS was chosen for experiments at many speed areas with load. The CB-MRAS gave acceptable performance at tested speeds. However, at lowest speed with load, relative speed difference is largest. More robust or sophisticated algorithms such as sliding mode theory, artificial intelligence should be developed for parameter IM identification and speed estimation at low and very low speeds. The methods for increasing the switching frequency, and dead-time compensation of power electronics devices should be utilized. The active load unit with large torque range should be constructed.

Acknowledgment

The paper was supported by the projects: Center for Intelligent Drives and Advanced Machine Control (CIDAM) project, reg. no. TE02000103 funded by the Technology Agency of the Czech Republic, project reg. no. SP2018/162 funded by the Student Grant Competition of VSB–Technical University of Ostrava.

References

- [1] ORLOWSKA-KOWALSKA, T. and M. DYBKOWSKI. Stator-Current-Based MRAS Estimator for a Wide Range Speed-Sensorless Induction-Motor Drive. *IEEE Transactions on Industrial Electronics*. 2010, vol. 57, iss. 4, pp. 1296–1308. ISSN 0278-0046. DOI: 10.1109/TIE.2009.2031134.
- [2] BRANDSTETTER, P. and M. DOBROVSKY. Speed Estimation of Induction Motor Using Model Reference Adaptive System with Kalman Filter. *Advances in Electrical and Electronic Engineering*. 2013, vol. 12, no. 1, pp. 22–28. ISSN 1336-1376. DOI: 10.15598/aeec.v11i1.802.
- [3] ALONGE, F., F. D'IPPOLITO, A. FAGIOLINI and A. SFERLAZZA. Convergence Analysis of Extended Kalman Filter for Sensorless Control of Induction Motor. *IEEE Transactions on Industrial Electronics*. 2015, vol. 62, iss. 4, pp. 2341–2352. ISSN 0278-0046. DOI: 10.1109/TIE.2014.2355133.
- [4] GACHO, J. and M. ZALMAN. IM Based Speed Servodrive with Luenberger Observer. *Journal of Electrical Engineering*. 2010, vol. 61, iss. 3, pp. 149–156. ISSN 1335-3632. DOI: 10.2478/v10187-011-0021-8.
- [5] NAYEEM HASAN, S. M. and I. HUSAIN. A Luenberger–Sliding Mode Observer for On-line Parameter Estimation and Adaptation in High-Performance Induction Motor Drives. *IEEE Transactions on Industry Applications*. 2009, vol. 45, iss. 2, pp. 772–781. ISSN 0093-9994. DOI: 10.1109/TIA.2009.2013602.
- [6] COMANESCU, M. Design and Implementation of a Highly Robust Sensorless Sliding Mode Observer for the Flux Magnitude of the Induction Motor. *IEEE Transactions on Energy Conversion*. 2016, vol. 31, iss. 2, pp. 649–657. ISSN 0885-8969. DOI: 10.1109/TEC.2016.2516951.
- [7] BRANDSTETTER, P. Sensorless Control of Induction Motor Using Modified MRAS. *International Review of Electrical Engineering*. 2012, vol. 7, iss. 3, pp. 4404–4411. ISSN 1827-6660.
- [8] GADOUE, S. M., D. GIAOURIS and J. W. FINCH. Sensorless Control of Induction Motor Drives at Very Low and Zero Speeds Using Neural Network Flux Observers. *IEEE Transactions on Industrial Electronics*. 2009, vol. 56, iss. 8, pp. 3029–3039. ISSN 0278-0046. DOI: 10.1109/TIE.2009.2024665.
- [9] TOLIYAT, H. A., E. LEVI and M. RAINA. A Review of RFO Induction Motor Parameter Estimation Techniques. *IEEE Transactions on Energy Conversion*. 2003, vol. 18, iss. 2, pp. 271–283. ISSN 0885-8969. DOI: 10.1109/TEC.2003.811719.
- [10] VASIC, V., S. N. VUKOSAVIC and E. LEVI. A Stator Resistance Estimation Scheme for Speed Sensorless Rotor Flux Oriented Induction Motor Drives. *IEEE Transactions on Energy Conversion*. 2003, vol. 18, iss. 4, pp. 476–483. ISSN 0885-8969. DOI: 10.1109/TEC.2003.816595.

- [11] KARANAYIL, B., M. F. RAHMAN and C. GRANTHAM. Online Stator and Rotor Resistance Estimation Scheme Using Artificial Neural Network for Vector Controlled Speed Sensorless Induction Motor Drive. *IEEE Transactions on Industrial Electronics*. 2007, vol. 54, iss. 1, pp. 167–176. ISSN 0278-0046. DOI: 10.1109/TIE.2006.888778.
- [12] MAOUCHE, A., M. M'SAAD, B. BENSAKER and M. FARZA. High Gain Adaptive Observer Design for Sensorless State and Parameter Estimation of Induction Motors. *International Journal of Control, Automation and Systems*. 2015, vol. 13, iss. 5, pp. 1106–1117. ISSN 1598-6446. DOI: 10.1007/s12555-014-0140-2.
- [13] VO, H. H., P. BRANDSTETTER, C. S. T. DONG and T. C. TRAN. Speed Estimators Using Stator Resistance Adaption for Sensorless Induction Motor Drive. *Advances in Electrical and Electronic Engineering*. 2016, vol. 14, iss. 3, pp. 267–273. ISSN 1336-1376. DOI: 10.15598/aeee.v14i3.1732.
- [14] CAO, P., X. ZHANG and S. YANG. A Unified-Model-Based Analysis of MRAS for Online Rotor Time Constant Estimation in an Induction Motor Drive. *IEEE Transactions on Industrial Electronics*. 2017, vol. 64, iss. 6, pp. 4361–4371. ISSN 0278-0046. DOI: 10.1109/TIE.2017.2668995.
- [15] ALEXANDER, C. and M. SADIKU. *Fundamentals of Electric Circuits*. New York: McGraw-Hill, 2005. ISBN 978-00-729-7718-3.
- [16] VACLAVEK, P. *Speed Estimation for AC Induction Machine Sensorless Control*. Brno, 2006. Habilitation Thesis. Brno University of Technology.
- [17] POPOV, V. M. *Hyperstability of Control Systems*. Berlin: Springer Verlag, 1973. ISBN 978-3-642-65656-9.
- [18] KHALIL, H. K. *Nonlinear Control*. London: Pearson Education, 2015. ISBN 978-0-133-49926-1.
- [19] KUBOTA, H., K. MATSUSE and T. NAKANO. DSP-Based Speed Adaptive Flux Observer of Induction Motor. *IEEE Transactions on Industry Applications*. 1993, vol. 29, iss. 2, pp. 344–348. ISSN 0093-9994. DOI: 10.1109/28.216542.

About Authors

Hau Huu VO was born in Binh Thuan, Vietnam. He received his M.Sc. degree in Automation Engineering from Ho Chi Minh City University of Technology in 2009, and Ph.D. degree in Electrical Engineering from VSB-Technical University of Ostrava in 2017. His research interests include robotics, control theory and modern control methods of electrical drives.

Pavel BRANDSTETTER was born in Ostrava, Czech Republic. He received his M.Sc. and Ph.D. degrees from Brno University in 1979 and 1987, respectively. He is now full professor and dean of Faculty of Electrical Engineering and Computer Science at VSB-Technical University of Ostrava. His research interests include AC controlled drives, sensorless control and applications of observers, estimator and soft computing methods in the control of electrical drives.

Thinh Cong TRAN was born in Da Nang City, Vietnam. He received his M.Sc. degree in Electrical and Electronic Engineering from Ho Chi Minh City University of Technology in 1998. His research interests include microcontroller systems and modern control methods of electrical drives.

Chau Si Thien DONG was born in Ho Chi Minh City, Vietnam. She received her M.Sc. degree in Automatic Control from Ho Chi Minh City University of Technology in 2003, and Ph.D. degree in Electrical Engineering from VSB-Technical University of Ostrava in 2017. Her research interests include nonlinear control, adaptive control, robust control, neural network and electrical drives.